ADMINISTRATIVE INFORMATION

1. **Project Name:** Low Temperature Reduction of Alumina Using Fluorine Containing Ionic Liquids

2. **DOE Award No:** DE-FC36-02ID14397

3. **Lead Organization:** The University of Alabama
PO Box 870202,
Tuscaloosa, AL 35487-0202

4. **Principal Investigator:** Dr. Ramana G. Reddy
Phone (205) 348-4246, fax (205) 348-2164
Email: rreddy@eng.ua.edu

5. **Project Partners:**

University of Kentucky	Dr. B. K. Parekh
Albany Research Center	Dr. William D. Riley
Century Aluminum	Dr. Frank Arnold
SECAT	Dr. Subodh K. Das

6. **Date Project Initiated:** 9/1/2002

7. **Completion Date:** 08/31/2007

Project Life Cycle
[ ] First Year
[ ] On-Going
[×] Final Year

AUTHORIZED DISTRIBUTION LIMITATION NOTICE

All information submitted in this report is public information. This report may be posted on the appropriate sub-program website, minus budget information.

EXECUTIVE SUMMARY

The major objective of the project is to establish the feasibility of using specific ionic liquids capable of sustaining aluminum electrolysis near room temperature at laboratory and batch recirculation scales. It will explore new technologies for aluminum and other valuable metal extraction and process methods. The new technology will overcome many of the limitations associated with high temperatures processes such as high energy consumption and corrosion attack. Furthermore, ionic liquids are non-toxic and could be recycled after purification, thus minimizing extraction reagent losses and environmental pollutant emissions.

Ionic liquids are mixture of inorganic and organic salts which are liquid at room temperature and have wide operational temperature range. During the last several years, they were emerging as

novel electrolytes for extracting and refining of aluminum metals and/or alloys, which are otherwise impossible using aqueous media. The superior high temperature characteristics and high solvating capabilities of ionic liquids provide a unique solution to high temperature organic solvent problems associated with device internal pressure build-up, corrosion, and thermal stability. However their applications have not yet been fully implemented due to the insufficient understanding of the electrochemical mechanisms involved in processing of aluminum with ionic liquids.

Laboratory aluminum electrodeposition in ionic liquids has been investigated in chloride and bis (trifluoromethylsulfonyl) imide based ionic liquids. The electrowinning process yielded current density in the range of 200-500 A/m^2, and current efficiency of about 90%. The results indicated that high purity aluminum (>99.99%) can be obtained as cathodic deposits. Cyclic voltammetry and chronoamperometry studies have shown that initial stages of aluminum electrodeposition in ionic liquid electrolyte at 30°C was found to be quasi-reversible, with the charge transfer coefficient $\alpha = 0.40$. Nucleation phenomena involved in aluminum deposition on copper in $AlCl_3$-BMIMCl electrolyte was found to be instantaneous followed by diffusion controlled three-dimensional growth of nuclei. Diffusion coefficient (D_o) of the electroactive species $Al_2Cl_7^-$ ion was in the range from 6.5 to 3.9×10^{-7} $cm^2\cdot s^{-1}$ at a temperature of 30°C.

Relatively little research efforts have been made toward the fundamental understanding and modeling of the species transport and transformation information involved in ionic liquid mixtures, which eventually could lead to quantification of electrochemical properties. Except that experimental work in this aspect usually is time consuming and expensive, certain characteristics of ionic liquids also made barriers for such analyses. Low vapor pressure and high viscosity make them not suitable for atomic absorption spectroscopic measurement. In addition, aluminum electrodeposition in ionic liquid electrolytes are considered to be governed by multi-component mass, heat and charge transport in laminar and turbulent flows that are often multi-phase due to the gas evolution at the electrodes. The kinetics of the electrochemical reactions is in general complex. Furthermore, the mass transfer boundary layer is about one order of magnitude smaller than the thermal and hydrodynamic boundary layer ($ReL\approx10{,}000$). Other phenomena that frequently occur are side reactions and temperature or concentration driven natural convection. As a result of this complexity, quantitative knowledge of the local parameters (current densities, ion concentrations, electrical potential, temperature, etc.) is very difficult to obtain. This situation is a serious obstacle for improving the quality of products, efficiency of manufacturing and energy consumption.

The gap between laboratory/batch scale processing with global process control and nanoscale deposit surface and materials specifications needs to be bridged. A breakthrough can only be realized if on each scale the occurring phenomena are understood and quantified. Multiscale numerical modeling nevertheless can help to bridge this gap. In conjunction with various scale experimental efforts, this project was aim to construct the basis for a strategy for innovation, by developing a generally applicable modeling methodology for understanding and controlling the electrochemical processes of aluminum electrodeposition in ionic liquids with the unifying characteristic that they are based on charge-driven mass transfer. The approaches developed in this project will not only be essential for the mass production of aluminum on any pilot scale or industrial level production processes, leading to the development of a new aluminum production

technology, but also bring significant benefits to the society in terms of saving energy, reducing pollutants emission and recovering valuable metals.

ACTUAL ACCOMPLISHEMENT

1. Project Objective:

The original goal of this R&D project is to develop a low temperature reduction process for the production of primary aluminum using chloride ionic liquids.

2. Tasks Accomplished:

The major objectives accomplished for this project include:

- Synthesized different chloride based and fluoride based ionic liquids.
- Determined physicochemical and thermodynamic properties of ionic liquids.
- Evaluated aluminum oxides and halides solubility in ionic liquids at various conditions.
- Performed lab and batch scale electrolysis experiments in controlled atmospheres and compared the process efficiency with industrial practice.
- Developed mathematical models for process parameters optimization and scaling-up.

The intense experimentation on solubility investigation revealed the synthesized ionic liquids have limited ability to dissolve aluminum oxide. This major obstacle encountered during this project resulted in project change as described in following section.

3. Project Changes:

Based on the recommendations from the Aluminum IOF review 2004, the project pathway has been modified. The primary focus of the project has been directed towards electro-refining of aluminum scrap using chloride ionic liquid electrolytes and reduction of aluminum from $AlCl_3$ using chloride based ionic liquid electrolytes.

4. Additional Accomplishments after Project Change:

The project partners recognized that development of a low temperature electrolytic process for reduction of aluminum chloride to produce aluminum would addresses the needs of the aluminum industry as stated in the aluminum industry roadmap. The partners undertook a program to:

(1) Experimental investigation of aluminum reduction from $AlCl_3$ using chloride ionic liquids at low temperatures.
(2) Electro-refining aluminum scrap using chloride ionic liquids at low temperatures.
(3) Carry out detailed evaluation and optimization of the experimental variables involved in the electrolytic process.
(4) Evaluated the morphology, structure and chemical composition of aluminum deposits using various characterization techniques

(5) Compared costs, processing issues and performance of the new reduction and refining process.

These tasks have been accomplished using the significant expertise that the R&D team already possesses in industrial electrowinning, materials characterization, and fundamental understanding of the metallurgical principles involved in industrial reduction of aluminum alloys.

PROJECT ACTIVITY SUMMARY

The work accomplished was according to the planned milestone in the original proposal (CPS 1854). Besides the synthesis and characterization of ionic liquids and investigation of solubility of oxides and fluorides, most of the work was focused on the scaling-up and modeling aluminum electrowinning from chloride ionic liquid mixture at low temperatures. It is summarized as follows:

1. Synthesis and Characterization of Ionic Liquids

With aim to explore alternative ionic liquid solvents for reduction of aluminum source, several PF_6^-, HSO_4^- and Tf_2N^- based ionic liquids were synthesized at UA. Table 1 shows the different ionic liquid and their properties. These ionic liquids were characterization using NMR technique.

Table 1. Physical and chemical properties of synthesized ionic liquids

IONIC LIQUID	MP, (°C)	T_{ONSET}, (°C)	DENSITY, G/ML (25°C)	VISCOSITY (25°C)/CP
C_4mimTf_2N	-25	439	1.43	52
C_6mimTf_2N	N/A	N/A	1.429	69
C_6mimPF_6	-78 (TG)	438.7	1.29	363
C_8mimPF_6	-82 (TG)	416.1	1.25	425.2
C_4mimCl (BMIMCl)	41	254	1.08	N/A
C_6mimCl (HMIMCl)	-75(T_g)	253	1.03	716

Ionic liquids (di-alkyl imidazolium chlorides) are synthesized using quaternization and anion exchange method as reported in the literature. For synthesizing 1-butyl-3-methyl imidazolium chloride ([BMIM]Cl) ionic liquid, the starting materials 1-methyl imidazole (99.7%, Sigma Aldrich) and chlorobutane (99.9%, Sigma Aldrich) were refluxed in a round bottom flask at 70 °C for 48 hours with constant stirring. Constant temperature was maintained using a heating mantle and stirrer placed under the heating mantle. Since the reagents are immiscible with the halide salt product, they will form as a separate phase. In order to purify the halide product it is washed with ethyl acetate (99.8%, Sigma Aldrich). Moreover, the halide salts are generally denser than the solvents, so removal of excess solvent and starting material can be achieved by decantation. Finally, after the solvent is decanted, the excess solvent and residues of starting material can be removed by heating the salt under vacuum. It is essential not to heat the halide salts to temperatures greater than about 80°C, since overheating can result in a reversal of the

quaternization reaction. The final product crystallized at room temperature after vacuum evaporation drying procedure.

Similar procedure mentioned above was used for synthesizing 1-hexyl-3-methyl imidazolium chloride ([HMIM]Cl) ionic liquid. 1-methyl imidazole and chlorohexane were used as starting materials. However, crystallization was not observed in case of [HMIM]Cl at room temperature as its melting point (-6 °C) is below room temperature. All the Pyrex glassware used in synthesis and experimental work were purchased from Fisher Scientific Company.

Chloroaluminate melts are formed by mixing di-alkyl imidazolium chloride salts with $AlCl_3$ (99.9%, anhydrous, Alfa Aesar). $AlCl_3$ was used as received without further purification. The mixing of chemicals was performed under an inert atmosphere of dry nitrogen (or argon) in a glove box (Labconco Corp). The glove box was vented using laboratory vacuum and then filled with high purity nitrogen (or argon) and this was repeated twice to ensure low oxygen atmosphere. The mixing reaction is highly exothermic, necessitating an extra care to keep the temperature of mixture under control. Extreme temperature can cause decomposition and discoloration of the melt. Thus $AlCl_3$ is added in small amounts to imidazolium salt, which allows heat dissipation. Careful weighing of the components can yield melts of precise composition with predetermined physical properties. All the mixing and weighing were done in the controlled atmosphere glove box. Chloroaluminate melts used in the present research are $AlCl_3$-[BMIM]Cl and $AlCl_3$-[HMIM]Cl.

The characterization of synthesized ionic liquids includes coulometric titration and nuclear magnetic resonance (NMR) analyses.

Coulomb Titration

Generally, the most common impurity likely to be present in ionic liquids is water. The removal of other volatile reaction solvents can be easily achieved by heating the ionic liquid under vacuum. The Coulometric titration method is used in this research to determine the moisture content of ionic liquids samples. This method uses iodine at the wire mesh of the generator electrode. When electricity is conducted across the mesh, one mole of the created iodine consumes one mole of water. One milligram of water is equivalent to 10.71 coulombs of electricity. The titration apparatus measures the electrical current needed to create iodine and remove the existing water. By employing a stepped pulse current, the apparatus can automatically selects titration speed depending on the amount of water present. At the end of titration the water content can be calculated by subtracting background drift.

Calibration were carried out using water standard 0.1 and 1.0 (Sigma-Aldrich, Germany) before titration. Each sample was at least 3 ml and repeated measurements were performed on each sample to ensure the deviation of results fall into the range of ±5%. The measurement showed that the water content of dried samples are less than 0.1 wt.% after drying. The sample without drying contained more water and its water content increases when exposed to humidity environment.

NMR Analysis

NMR spectroscopy is an essential analytical tool for determining chemical structure and dynamics of organic solvents. The chemical shifts of proton (^{1}H) and carbon-13 (^{13}C) NMR are the most common and versatile analytic methods to reveal the environmental on the nucleus. The degree of dissociation of ionic liquids will create different electron densities on the atoms, which would be the potential ionic state. With NMR investigation on the chemical shifts of the imidazolium salts function on the anions, alkyl group lengths, solvents and concentration, it is possible to know the outcome of different solvent reactions and purity levels of ionic liquid sample. The NMR spectra for the synthesized ionic liquids compared well with that reported in literature. The NMR spectrum results for [HMIM]Cl are as follows: ^{1}H NMR results: δ 0.84 (t), 1.20 (sextet), 1.74 (q), 3.88 (s), 4.21 (t), 7.88 (s), 7.97 (s), 9.74 (s). ^{13}C NMR (DMSO, ppm) results: δ 13.16, 18.64, 31.32, 35.58, 48.23, 122.21, 123.44, and 136.75.

^{1}H and ^{13}C NMR spectra were obtained at ambient temperature on a Bruker AM-500 spectrometer (Houston, TX). Chemical shifts relative to tetramethylsilane (TMS) were calculated with chloroform ($CHCl_3$) as an internal standard. An insert tube filled with D_2O was used for the locking and referencing and the spectra were processed using MestRe-C® v4.51 (Mestrelab Research, Spain). The NMR spectra of neat sample were broader than those in chloroform solvents because of the high viscosity of ionic liquid samples.

2. Solubility of Al_2O_3 in Ionic Liquids

The process of obtaining a metal from its oxides by electrolysis was pioneered by the Hall-Herault process of aluminum electrowinning. Since then, it has been well established that in halide electrolytes, only the dissolved oxides are available for the dissociation at the electrode to release the metal during electrolysis. Therefore, the solubility of the aluminum oxide in the ionic liquid electrolytes is an important parameter which determines the economical and technical viability of the molten salt electrolysis process.

The industry practices in recovery of aluminum metal is divided into two steps: the production of pure alumina (Bayer Process); and its molten salt electrolysis, using molten cryolites(Na_3AlF_6) in which aluminum oxide Al_2O_3 has been dissolved(solubility: about 5%). The cryolite electrolysis process has been the most widely used and still accounts for about 90% of the total production of aluminum since 1886. Unfortunately, these processes have severe environmental problems and are extremely energy intensive. High temperature electrolysis (900-1000^{o}C) inevitably has high production costs and pollutants emission. In contrast, if aluminum oxide can be dissolved in ionic liquids to some extent and therefore doing the electrolysis at ambient temperature. The existing problems of cryolite electrolysis processes will be easily avoided. Up to now, few research works has been done concerning the solubility of Al_2O_3 in ionic liquids.

The experiments on the solubility studies were conducted in a sealed glove box filled with inert gas (UHP nitrogen) to prevent moisture. The solubility levels of Aluminum oxide in the electrolyte were studied by measuring the EMF between a reference and working electrode immersed in the electrolyte. This technique is based on simple electrochemical principle. When two different electrodes, while one contained in a separated chamber to avoid the mass transfer

(in this case, it is the reference electrode), are immersed in the electrolyte, the potential difference between them varies with the concentration of the dissolved ionic species. When the concentration of the dissolved species reaches the maximum solubility limit (i.e. saturation) in the electrolyte, the EMF between the electrodes will attain a stable value.

After the electrolyte mixture reached the required constant temperature, the reference and the working electrodes were lowered into the molten electrolyte and allowed to remain until the cell reached a constant potential measured between the electrodes. The EMF can be measured using digital multimeter. After the equilibrium is reached, the aluminum oxide is added in weighed quantities to the electrolyte. The voltages are measured after each addition. Electromotive forces are allowed to stabilize for every addition and these stable voltages are recorded. The quantity of the aluminum oxide added until the point beyond which the EMF became stable is the solubility level of the oxide in ionic liquid electrolyte at the given temperature. Table 2 further compared the solubility data determined by both methods for C_6mimPF_6 and C_8mimPF_6 ionic liquids. It can be seen that Dipping method showed higher solubility than EMF method because the precipitated oxide powder into ionic liquids is counted as dissolving.

Table 2. Al_2O_3 solubility experimental preliminary results

Temp.		Dipping method*				EMF method		
		g/ml	wt %	Time	IL wgt. loss (%)	g/ml	wt %	Final emf (V)
C_6mimPF_6	100°C	0.0068	0.5399	18 hrs	0.75	0.0002	0.0155	0.65~0.70
		0.00193*	0.1610*	18 hrs	2.11*			
	150°C	0.0166	1.30	18 hrs	1.05	N/A	N/A	N/A
		0.00212*	0.1782*	18 hrs	2.35*			
C_8mimPF_6	100°C	0.0045	0.3553	18 hrs	0.98	0.00016	0.0131	0.014-0.015
	150°C	0.0089	0.7026	18 hrs	1.23	N/A	N/A	N/A

*MgO solubility data

3. Solubility of Fluorides in Ionic Liquids

The experimental apparatus was a Model 340 Spectrophotometer which combines both transmittance and absorbance measurements with wavelength range from 330 to 1000 nm. The monochromator on the spectrophotometer consists of a plane diffraction grating in an f7 Ebert mounting with first surface reflective optics. The transmittancy and absorpbancy measurement of pure dehydrated C_6mimPF_6 were conducted using clean Fisherbrand disposable cuvettes (13×100mm). Cuvette with distilled water was used as the 0 and 100 references for absorpbancy and transmittancy values respectively.

Anhydrous AlF_3 (-100 mesh) and $MgCl_2$ (-100 mesh) were purchased from Fisher Scientific, 99.9% and used without further purification. The powder of AlF_3 and $MgCl_2$ were mixed with dehydrated C_6mimPF_6 on stirring hot plate at 200^oC for 2 hours. Before absorptancy and transmittancy measurements, each cuvette sample was kept still about half an hour for cooling down to room temperature. As shown in the Transmittance and Absorbance spectra for C_6mimPF_6, an extremely weak band occurs at about 500 nm. Additional bands are observed at about 850 nm.

In order to determine the unknown concentration of fluorides dissolved in ionic liquids, the choice of wavelength for quantitative analysis is critical. Factors which influence the choice include: (1). Wavelength errors, (2). Transmittancy errors, (3) solution effects, (4) magnitude of absorbancy coefficient, (5) resolution, and (6) effect of impurities. By reviewing all above six factors, 520 nm and 850 nm were chose for concentration determination (factor 4 favors the absorption maximum, 1 and 5 favors absorption minimum or maximum).

By plotting the absorpbancy for a standard stray light filter (420-890nm) versus concentration, it is straightforward to determine which curve follows Beer's law. For both AlF_3 and $MgCl_2$, 850 nm is used to determine the unknown concentration quantitatively. It was found that C_6mimPF_6 maximum absorbancy for AlF_3 is approximately 16 g/l (0.191 mol/L) at room temperature, C_6mimPF_6 maximum absorbancy for $MgCl_2$ is approximately 19 g/l (0.200 mol/L) at room temperature.

4. Aluminum Electrowinning in Ionic Liquids

Laboratory and batch recirculation of aluminum electrolysis in ionic liquids were investigated in chloride based ionic liquids. The chloride ionic liquids C_6mimCl mixed with $AlCl_3$ comprised the electrolytes in which aluminum electrowinning was investigated. The results revealed that large scale aluminum reduction is feasible in chloride ionic liquids. The experimental parameters such as temperature, applied cell voltage, electrolyte composition investigated were based on previous laboratory studies. The experimental setup consisted of three parts; electrolyte reservoir, pump and electrowinning cell. The purpose of separating electrolyte mixing from electrowinning process was to investigate the feasibility of aluminum electrowinning in continuous or batch mode for scale-up of the process.

Anode Effects

Consumable graphite anode was used as both cathode and anode in industrial process of manufacturing electrolytic aluminum by electrolysis of cryolite melts at 900-1000^oC. The electrolysis at low temperatures (30-120^oC) in ionic liquids provided an advantage of protecting the graphite anode from electrochemical corrosion in addition to heat energy saving compared with cryolite electrolysis at high temperatures. In this work, electrolysis in ionic liquids at 80-90^oC were done on a bath recirculation process using resin impregnated graphite and extruded carbon anode. The resin impregnated graphite and YBD extruded carbon which both are reinforced for better mechanic strength and manufactured particularly for electrolysis in chloride or fluoride electrolytes. The extruded carbon anode was reused twice in the batch electrowinning and still showed good current density behavior and negligible weight losses. But the resin

impregnated graphite anode had more than 10 wt % loss after 2 hrs electrowinning. It was not reusable since it appeared to be significantly dissociated in shape and did not show comparable current density with that of first usage. Thus most of the batch recirculation electrowinning experiments were conducted using extruded carbon anode unless specified otherwise.

The extruded carbon anode has better mechanical properties, larger porosity and particle size, but less electrical conductivity than resin impregnated graphite. It should be noted that the average current density during electrowinning for these two anodes did not show much differences. This is because ionic liquid electrolyte has much less electrical conductivity (in the range of 5-10 mS/cm) than graphite and carbon anodes (~1.3×10^6 mS/cm) as reported in literature. The conductivity improvement on anodes would not contribute significantly to the current density of electrowinning process. Nevertheless, the extruded carbon electrode in a chloride ionic liquid bath was found to work for a longer time with less passivation and degradation during electrolysis due to the better electrochemical stability. These results showed that the extruded carbon electrode can be used for large-scale aluminum electrowinning from ionic liquid electrolytes at studied temperature ranges.

Effects of Applied Cell Voltage and Electrolyte Flow Rate

The batch scale electrowinning experiments under different experimental conditions showed that the highest average current density and current efficiency were obtained at 3.5 V and 20 mL/min for applied cell voltage and flow rate, respectively. When increasing the recirculation rate of electrolyte and cell voltage with same initial concentration, both current densities and current efficiencies were improved. The effects of applied cell voltage were observed earlier in our laboratory electrowinning experiments. The increase in current density with applied cell voltage is possibly due to the polarization. Moreover, with the increase in voltage the rate of discharge at the cathode increases as a result current density, which is the measure of rate of discharge, also increases. The higher current efficiencies indicate that the dominant reduction reaction taking place at cathode is the reducing of aluminum ions at higher voltages. The effect of electrolyte flow rate showed that convection of electrolyte is another important factor that needs to be considered during scaling up of the present process to larger scale electrowinning processes. Results of laboratory electrowinning experiments also showed same trend in current density. This might contribute to the decrease of diffusion layer thickness at the cathode surface caused by high flow rate.

A similar variation of current density with time was observed for all conducted batch experiments. Current density drops suddenly when electrolysis starts and gradually keeps stable after 2-3 minutes. Passivation of anode in electrolyte especially in high viscosity ionic liquid electrolyte might contribute to the initial current density loss at the beginning of electrowinning. The high contact resistance at the graphite anode interface and the large charge transfer resistance at electrode/electrolyte interface are most probably associated the poor wettability of the ionic electrolyte with the graphite or carbon anode. In the porous electrode, the high viscous ionic liquid cannot effectively wet the graphite particles covered by PVDF. This phenomenon was also obvious in the current density variation curves for resin impregnated graphite and extruded carbon anodes. Extruded carbon was more porous than resin impregnated graphite and thus showed larger initial current density drops. Addition of the organic solvent may help to

improve the wettability of the electrolyte with the electrode. The decrease of the electrolyte viscosity can speed the diffusion of ions and promotes the electrode/electrolyte wettability.

Characterization of Deposit

Our early laboratory experiments studied the evolution of deposited grain size and morphology with different temperatures and current densities. It was found that the increase in temperature tends to produce fine-grained deposit and the deposited particles become coarser when current density increases from $50A/m^2$ to $100A/m^2$. However, the electrowinning time and electrolyte flow rate, which are among other important factors that affect the grain size and morphology of deposits, were kept constant during these studies. In this work, the effects of deposition time and electrolyte flow rate were investigated under constant temperature and applied cell voltage.

The SEM images of the aluminum deposits obtained from different electrowinning time (1 and 2 hours) and flow rates (5 and 20 ml/min) showed that that there were no significant size or morphology differences with different flow rates (stagnant, 5mL/min and 20 mL/min) when the electrowinning time was 1 hour. When the time increased to 2 hours, deposited grains were agglomerated together and grew bigger than those of 1-hour deposition. In the meanwhile, higher flow rate tends to yield more agglomeration and clusters than lower flow rate and stagnant conditions. This phenomenon is consistent with our early laboratory results since the current density increases with electrolyte flow rate. With increase of current density, agglomeration of particles can also be observed in deposit in laboratory experiments [8]. Deposited particles grew together and formed clusters rather than separated particles. Low current density leads to a uniform deposition, while high current density resulted in agglomerating and clustering.

The driving force for migration of reducible ions is low at low current density and so the growth rate of metal nuclei is lower than that of higher current density. As a result, the deposit tends to grow in a uniform way, leading to smoother and finer grained deposition, and a reduced tendency for forming anomalous or clustered metal deposition. As current density increases, the growth rate of nuclei increases and the deposit becomes coarse-grained. When the current density continues to increase to some degree at which the forming rate of new nuclei is greater than the growth rate of existing nuclei. Deposited grain particles begin to attach to one another and form cluster structure.

Pilot Scale Electrowinning

Large scale electrowinning experiments are necessary for industrial application. Design of pilot electrowinning cell should take into consideration of important parameters optimized by laboratory and batch recirculation experiments. The prototype of one of the pilot cells with volume of 5 liters has been set up according to previous experimental and modeling studies as shown in Figure 1. Future electrowinning experiments based on this type of pilot cells can provide valuable information concerning scaling-up applications.

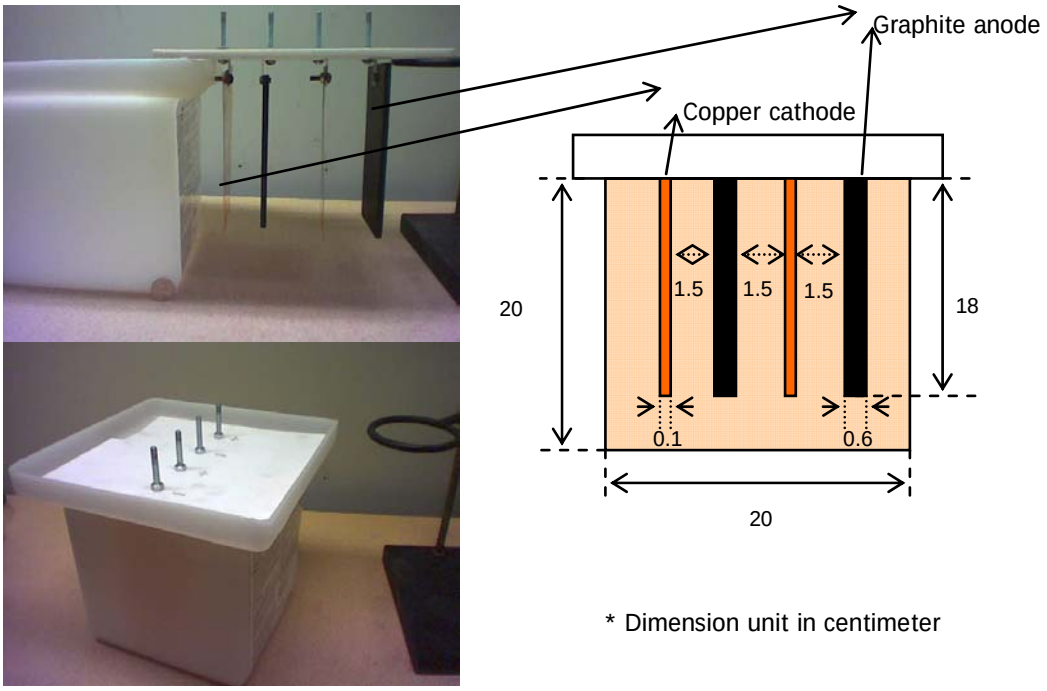

Figure 1. Pilot aluminum electrowinning experiment setup.

PRODUCTS DEVELOPED UNDER AWARD AND TECHNOLOGY TRANSFER

Journal Papers:

1. M. Zhang, V. Kamavaram, and R. G. Reddy, "New Electrolytes for Aluminum Production: Ionic Liquids", *JOM*, 11, p. 54-57, 2003.
2. V. Kamavaram, D. Mantha, R. G. Reddy, "Electrorefining of Aluminum Alloy in Ionic Liquids at Low Temperatures," *Journal of Mining and Metallurgy,* vol. 39(1-2) B, pp. 43-58, 2003.
3. M. Zhang, V. Kamavaram, and R. G. Reddy, "Thermodynamic Properties of 1-butyl-3-methylimidazolium chloride (C_4mim[Cl]) Ionic Liquid," *Journal of Phase Equilibria and Diffusion,* Vol. 26(2), pp.124-130, 2005.
4. V. Kamavaram, D. Mantha, R. G. Reddy, "Recycling of Aluminum Metal-Matrix Composites using Ionic Liquids at Low Temperatures," *Electrochimica Acta,* vol. 50(16-17), pp. 3286-3295, 2005.
5. M. Zhang, V. Kamavaram and R. G. Reddy, "Ionic Liquid Metallurgy: Novel Electrolytes for Metals Extraction and refining Technology", *Minerals & Metallurgical Processing,* Vol. 23 (4), pp. 177-186, 2006.
6. V. Kamavaram and R. G. Reddy, "Thermal Stabilities of Di-alkylimidazolium Chloride Ionic Liquids", *International Journal of Thermal Sciences,* Vol. 47, pp.773-777, 2008.

Conference Papers/Proceedings

1. V. Kamavaram and R. G. Reddy, “Physical and Thermal Properties of Ionic Liquids Used in Aluminum Electrorefining at Low Temperatures,” Aluminum 2003, ed. S. K. Das, (Warrendale, PA: TMS, 2003), 299-307.
2. M. Zhang, V. Kamavaram and R. G. Reddy, “Application of Fluorinated Ionic Liquids in the Extraction of Aluminum”, Light Metals 2004, Ed. A.T. Tabereaux, TMS, Warrendale, USA, pp. 315-319, 2004.
3. V. Kamavaram and R. G. Reddy, “Aluminum Electrolysis in Ionic Liquids at Low temperature,” Metal Separation Technologies III, edited by R. E. Aune and M. Kekkonen, ECI 2004, p. 143-151, 2004.
4. M. Zhang, V. Kamavaram and R. G. Reddy, "Aluminum Electrowinning in Ionic Liquids at Low Temperature", Light Metals 2005, ed. Halvor Kvande, TMS, Warrendale, pp 583-588, 2005.
5. M. Zhang, R. G. Reddy, "Electrical Field and Current Density Distribution Modeling of Aluminum Electrodeposition in Ionic Liquid Electrolytes", ECS Trans. Vol. 1 (16), pp. 47-60, 2006.
6. M. Zhang and R. G. Reddy, "Aluminum Extraction Via Batch Recirculation Electrolysis in Ionic Liquids", Advanced Processing of Metals and Materials”, editors: F. Kongoli and R. G. Reddy, The Minerals, Metals and Materials Society (TMS), Warrendale, USA, Vol. 4, pp. 237-246, 2006.
7. M. Zhang, R. G. Reddy, "Recycling of Aluminum Alloy Waste via Ionic Liquid Electrolytes", Green Engineering for Materials Processing, eds. Heather Kaminsky, Sharon Marra, Carol Jantzen, Riad Asfahani, Materials Science & Technology, ASM International, Materials Park, Ohio, USA, MS&T’06 CD, pp. 153-161, 2006.
8. M. Zhang and R. G. Reddy, "Ionic Liquid Electrowinning of Aluminum – Modeling of Batch Reactor," Aluminum Reduction Technology: Cell Fundamentals, Phenomena and Alternatives, Light Metals, editor: Morten Sorlie, TMS, Warrendale, USA, pp. 385-390, 2007.
9. M. Zhang and R. G. Reddy, "Application of [C4min][Tf2N] Ionic Liquid as Thermal Storage and Heat Transfer Fluids," editor J. Weidner, ECS Transactions, Vol. 2 (28), pp. 27-32, 2007.
10. M. Zhang and Ramana G. Reddy, “Modeling of Low Temperature Aluminum Electrowinning in Chloroaluminate Ionic Liquid Electrolytes” Proceedings International Conference, Advances in Metallurgical Processes and Materials, National Metallurgical Academy, Ukraine, Dnipropetrovsk, Ukraine, Vol. 2, pp. 15-29, 2007.
11. M. Zhang and R. G. Reddy, “Evaluation of Ionic Liquids as Heat Transfer Materials in Thermal Storage Systems”, Energy: Energy Materials, editors: F. Dogan, M. Awano, D. Singh and B. Tuttle, ASM International, Materials Park, Ohio, USA MS&T’07, pp. 151-160, 2007.
12. M. Zhang and Ramana G. Reddy, “CO_2 Free Electrochemical Process for Production of Light Metals Using Ionic Liquids as Electrolytes”, Carbon Dioxide Reduction Metallurgy, editors: N. R. Neelameggham and R. G. Reddy, TMS, Warrendale, USA, pp. 161-170, 2008.

MODELING OF ALUMINUM ELECTROWINNING IN IONIC LIQUIDS

The preliminary mathematical modeling for aluminum electrowinning in ionic liquid electrolyte is described in the following paragraphs. The model utilizes the information capabilities of the Navier-Stokes equations written for the electrode (metal) and electrolyte media. The objectives of the transport modeling are as follows:

a) To facilitate advances in the application of ionic liquid electrolytes in aluminum electrowinning.
b) To better understand the physical and chemical processes of aluminum electrowinning in ionic liquid electrolytes.
c) To recommend the technology for electrowinning of aluminum in ionic liquid electrolytes for large-scale electrowinning processes.
d) To optimize the electrowinning operation so as to improve the stability of the process and to maximize metal yield.

The mathematical model includes calculation on electric field, fluid flow, concentrations of dissolved chemical species and temperature field. The solution procedures for the governing equations of the physical phenomena involved in the process are based on the principles of conservation of mass, momentum, energy and electric charge. The computational model can be used in fine-tuning of the process which may be very sensitive to the concentration of certain species.

System Description and Assumptions

There are generally three contributions to mass transport of electroactive species in electrolyte, namely diffusion, convection and migration. In the case of chloroaluminate ionic liquid electrolyte, the reactants ($AlCl_4^-$, $Al_2Cl_7^-$ and Cl^- etc.) are transported by a combination of convection and diffusion while $[HMIM]^+$ (or C_6mim^+) ions from the background electrolyte carry the migration current.

Figure 2 illustrates the schematic mechanism of aluminum electrodeposition in ionic liquid electrolyte. The vertical 2D cross section represents the cathode and anode electrodes located in Cartesian coordinate system. The mathematical model focuses on electrolyte surrounding planar copper cathode and graphite anode when applying a continuous direct current. The geometry of the model and the symbols used to designate its geometrical dimensions are shown in Figure 2. The electrolyte domain, Ω, is bound by inner and outer boundary surfaces, with length L_d and L_c or L_a, respectively. The cathode and anode are assumed to be situated at a distance far enough from each other to ensure that the electrode reaction products do not affect the electrolyte domain being studied. Transport of current is assumed to occur solely through the electrolyte fluid. Ionic liquid electrolyte is treated as a homogeneous solution. Some detailed assumptions are made in developing the model for electrodeposition process as follows,

a) The electrolyte is assumed to be binary with only Al ions as the electroactive species.
b) Isothermal conditions exist, and side reactions are neglected.
c) Possible bubble generation from the electrode surface is not considered.
d) A steady state laminar fluid is assumed, the velocity profile is fully developed at the electrode/electrolyte interface; in other words, there is no end effect.

e) Volume changes arising during cell operation are neglected.
f) Physical and transport properties are constant. Constant values for transference number and solution phase diffusivity are assumed at all times and at all points in the cell.

The mixed mass transfer coefficients or rate constants of aluminum deposition were sequentially determined in the laboratory cell under controlled electrodeposition conditions, assuming that the mass transfer coefficient is independent of current density, as shown in Table 3, Table **4** and Table 5. Other data were taken from literature as cited in the tables.

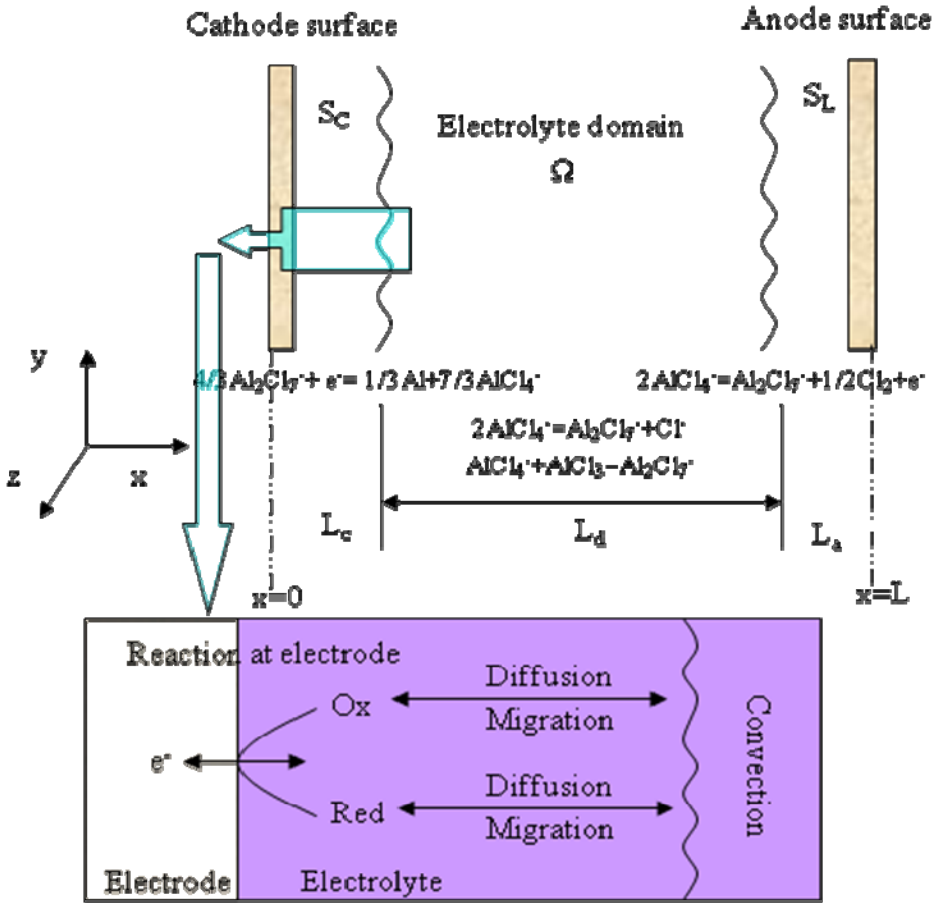

Figure 2. Planar geometry of aluminum electrodeposition in Cartesian coordinate system.

Table 3. Parameters and Material Constants used in Modeling

Properties (Room Temperature)	Electrode		[HMIM]Cl+$AlCl_3$ Electrolyte (50-50mol%)
	Copper Cathode	Graphite anode	
Density (kg/m^3)	8940	2250	1238
Electrical Resistivity (Wm)	1.68×10^{-8}	7.00×10^{-5}	~10
Specific Heat (J/kg K)	385	669	1800
Thermal Conductivity (W/K m)	295	24	0.186
Viscosity (c_p)	-		27
Electrical Conductivity (S/m)	-		0.1

Table 4. Standard potentials Kinetic parameters for reactions at cathode and anode.

Reactions	n_k	γ_{ik}	α_{ak}	α_{ck}	i_{0k}^{ref} (A/m^2)	E^0_k (Volts)
$4Al_2Cl_7^- + 3e^- = Al + 7AlCl_4^-$	3	0.7	0.5	0.5	10^{-5}	-0.5
$4AlCl_4^- = 2Al_2Cl_7^- + Cl_2 + 2e^-$	2	0.7	0.5	0.5	10^{-5}	2.50

Table 5. Transport properties of species in [HMIM]Cl-$AlCl_3$ mixture (at 25°C)

Species/Anions	C_6mim^+	$AlCl_4^-$	$Al_2Cl_7^-$	Cl^-
Reference concentration, $C_{i,ref} \times 10^3$ (mol/ml)	1	0.5	0.5	0.1
Diffusion Coeff., $D_i \times 10^5$ ($cm^2 s^{-1}$)	0.144	1.065	0.61	9.321
Mobility ($m_i = D_i/RT$) $\times 10^9$, $cm^2 mol\ J^{-1} s^{-1}$	0.581	4.30	2.46	37.6
Transport number, $t^{+/-}$	0.71	0.23	0.06	-
Density, g/m^3	-	1.294	1.389	1.234
Molecular weight, g/mol	-	279.96	413.22	-
Molar volume, V_{mol}, cm^3/mol	-	216.4	297.54	-
Conductivity, mS/cm	-	22.6	14.5	-

Geometry Model

Figure 3 shows the two dimensional (2D) meshed geometry of electrolytic cell with aspect ratio of 1:1. They are top view cross-sections of cylindrical and rectangular shape electrowinning cells. Figure 4 shows the three dimensional (3D) meshed geometry of cylindrical electrowinning cell. Ansys® Preprocessor was employed to construct the 2D and 3D geometries and mesh the domains. All the geometries are based on actual dimensions and aspect ratio of batch mode electrowinning cell used in experiments. The cell walls are treated as non-slip boundaries and infinite boundaries for fluid flow and electrical field calculation, respectively. An unstructured mesh was used to discretize the domain in order to convert the governing continuity and momentum equations to algebratic equations that can be solved mathematically.

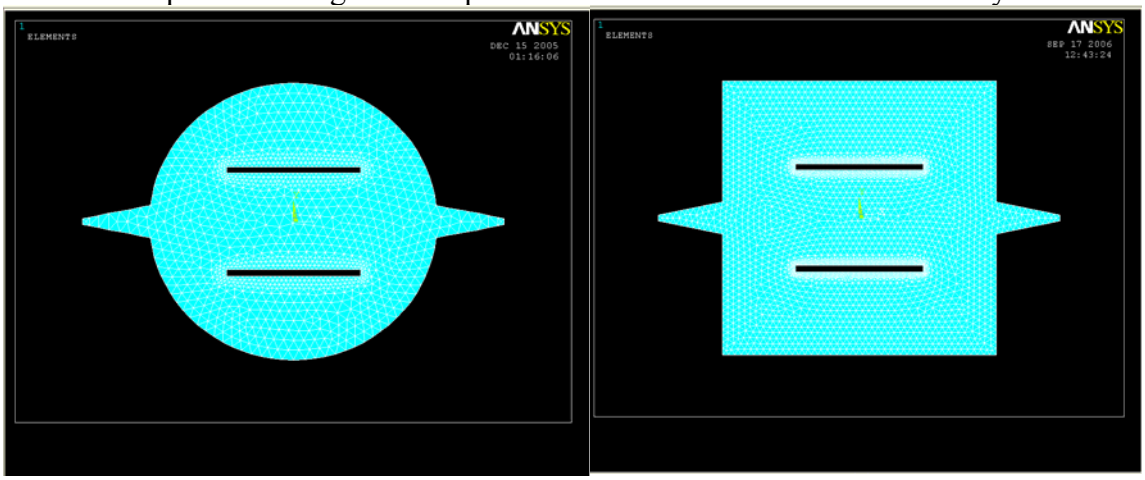

(a). Cylindrical cell (b). Rectangular cell

Figure 3. Non-structured 2-D meshing grid model of cross-section view of electrowinning cells.

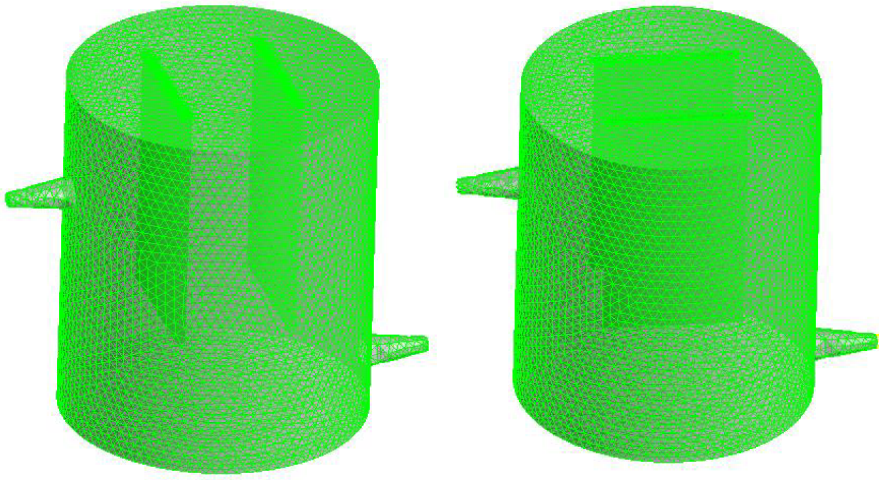

(a) Normal Configuration (b) Parallel configuration

Figure 4. Unstructured 3-D meshing of electrowinning cell.

Electrical Potential Models

Quasi-static electromagnetic field theory may apply to calculate the electrical field distribution over the extent of the cell device. The Maxwell's equations were used for electrostatic field analysis. By neglecting the time-derivative of magnetic flux density (the quasi-static approximation), the system of Maxwell's equations can be reduced to:

$$\nabla \times E = 0 \quad (1)$$

$$\nabla \cdot B = 0 \quad (2)$$

$$\nabla \cdot D = \rho' \quad (3)$$

The electric field E is irrotational, and the scalar potential equation can be defined by:

$$E = -\nabla \phi \quad (4)$$

The simplified constitutive equation for electromagnetic field without velocity effect:

$$D = \varepsilon E \quad (5)$$

Electric scalar potential equation for electrostatic analysis can be derived from above Maxwell's governing equation and constitutive equation:

$$-\nabla \cdot (\varepsilon \nabla \phi) = \rho' \quad \text{or} \quad \nabla \cdot (\nabla \phi) = \nabla^2 \phi = -\frac{\rho'}{\varepsilon} \quad (6)$$

This equation is also known as Poisson's equation. In regions of space where there is no charge density, the scalar potential satisfies Laplace's equation.

$$\nabla^2\phi = 0 \tag{7}$$

The Poisson equation relates the charge density to the Laplacian of the electric potential, as shown in Eq. 6. It can be solved with constant values of ϕ at the electrodes, and zero flux at the other boundaries by assuming electroneutrality (no charge density) in bulk electrolyte. However, the use of both Poisson's equation and electroneutrality could render inconsistence especially when it needs to determine the behavior of each species in the electrolyte near the electrodes. This is because the charge density in the electric double layer near the electrodes cannot be neglected. This double layer region has very large electric field and thus the electroneutrality may not be valid.

With the help of the Ohm's and Coulomb's Laws, it is possible to numerically solve the Poisson equation in 3-D domain;

$$i = -\kappa\nabla\Phi \tag{8}$$
$$\nabla\cdot\Phi = 0 \tag{9}$$

The partial current densities can be evaluated once the conductivity and potentials are known. The conductivity of the electrolyte can be calculated by the following equation.

$$\kappa = F^2\sum_{i=1}^{2} m_i C_{i,ref} \tag{10}$$

The solution technique requires the assumption of an initial current density distribution to calculate the bulk and surface concentrations along the electrode. The calculated concentrations are used to estimate a new current density distribution. Iterations continue until the new current distribution agrees with the previous values to within three decimal places.

Fluid Flow Modeling

Considering the flow of a viscous, electrically conducting, incompressible fluid subject to an electrical field, the fundamental physical laws applicable to the electrolyte fluid flow system are the Navier-Stokes equations. The expression for the electrolyte fluid motion is given by:

$$\rho\frac{\partial u}{\partial t} + \rho(u\cdot\nabla)u = -\nabla P + \mu\nabla^2 u + \rho g \tag{11}$$

The continuity equation which expresses conservation of the mass is given by:

$$\nabla\cdot(\rho u) = 0 \tag{12}$$

For the electro-hydrodynamic flow which is the case in electrowinning process, it is necessary to simultaneously solve for the transport of space charge and the electric field, in addition to the momentum equations and the mass conservation, i.e., the Navier-Stokes equation has to be

combined with Ohm's law and the conservation of charge equation as shown in Eq. 8 and 9. The methodology for solving this coupled problem is shown in Figure 5.

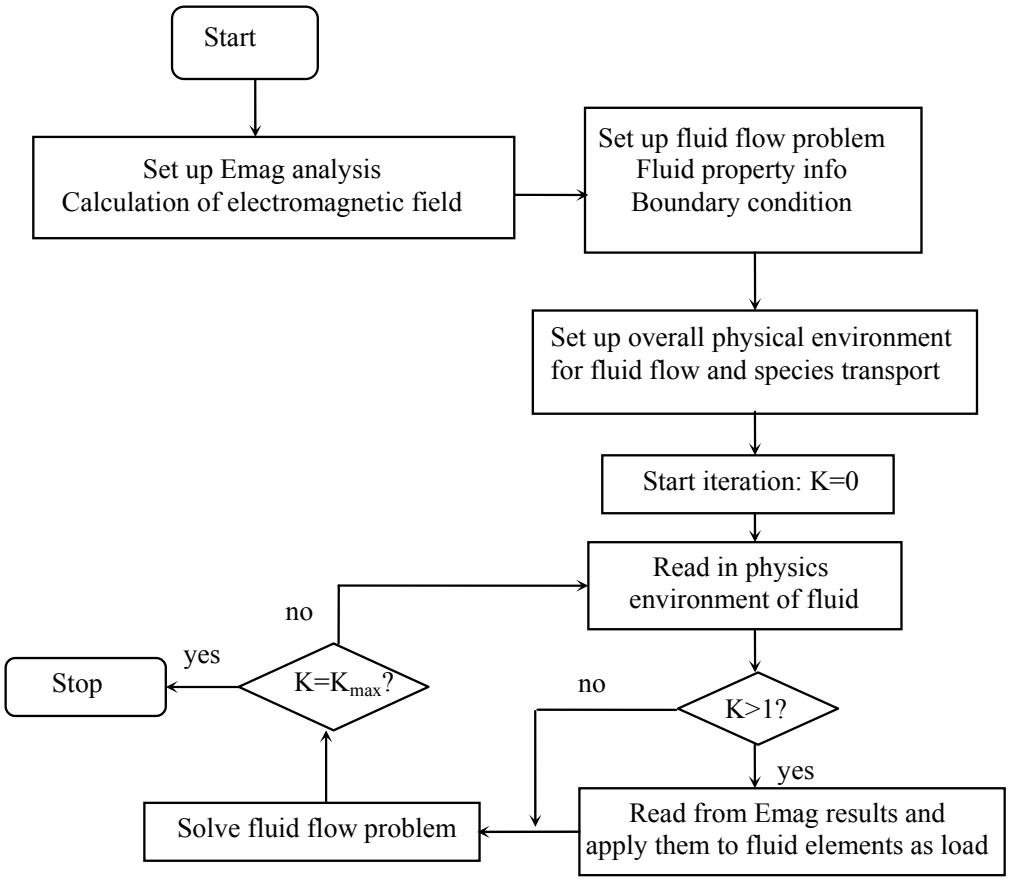

Figure 5. Modeling methodology of electrically and fluid flow coupled field in aluminum electrowinning.

Mass Transport in Bulk Electrolyte

The governing equations for species involve a mass transport for species i and the electroneutrality condition. The governing equations within the electrolyte domain include differential material balances for all species considered in the model. The conservation of species expression is given by:

$$\frac{\partial C_i}{\partial t} = D_i \nabla^2 C_i + \frac{z_i}{|z_i|} m_i \nabla \bullet (C_i \nabla \phi) \qquad (13)$$

where t denotes time, D_i is the diffusion coefficient, zi is the electrical charge number and mi is the ionic mobility of species i.

The electroneutrality condition in the electrolyte domain is given by:

$$\sum_i z_i C_i = 0 \tag{14}$$

The current density is determined by combining the Eqns. 13 and 14. The equation is given by:

$$i = -F\sum_i z_i D_i \nabla C_i - F\sum_i z_i^2 D_i \nabla \Phi \tag{15}$$

Electrode-Electrolyte Interface

Because electrode reactions which occur at the electrode-electrolyte interface play a major role in determining the electrochemical kinetics, knowledge of these reactions is critical in evaluating the process parameters such as current efficiency and current density. Species charges and solvent dipoles are arranged at the interface between electrode and electrolyte solution. The arrangement in the inter-phase region at the boundary of an electrode-electrolyte is termed as "electric double layer". Several models were proposed to describe electric double layer. These are: (a) Helmholtz compact layer model, (b) Gouy-Chapman diffuse layer model, and (c) Stern model. A more comprehensive model addressing the inter-phase phenomena in three-dimension is the Bockris-Devanathan-Muller (BDM) model. This triple layer model incorporates all the above three models. Because of the non-linear variation in the charge density within the electric double layer, the potential distribution is no longer governed by Laplace's equation. The charged species and potential distribution equations are coupled together. They have to be solved simultaneously in order to obtain the current density and potential distribution within the interface.

$$\rho' = \sum q_i c_j = \sum z_j e c_j \tag{16}$$

$$c_j = c_j^{\infty} \exp\left[-\frac{z_j e\phi_0}{k_B T}\right] \tag{17}$$

$$\nabla^2\phi = -\frac{\rho'}{\varepsilon} = -\frac{1}{\varepsilon}\sum z_j e c_j^{\infty} \exp\left[-\frac{z_j e\phi_0}{k_B T}\right] \tag{18}$$

Due to the complexity involved in solving the above Eqns. 16, 17, and 18, it was assumed that i = i_{0k}. The conductivity k was calculated using Eq. 10. The solution potential ϕ_o (at the cathode surface ϕ_{oc} and anode surface ϕ_{oa}) was calculated by substituting i and k into the Eq. 8. The equilibrium open-circuit potential E_k is given by Eq. 19. Then the reaction current density was calculated by Butler-Volmer equation 20.

$$E_k = E_k^0 - \frac{RT}{n_k F}\ln\prod_i\left(\frac{C_{i\infty}}{\rho}\right)^{s_{ik}} \tag{19}$$

$$i_k = i_{0k}^{ref}\prod_i\left(\frac{C_{i0}}{C_{iref}}\right)^{\gamma_{ik}} \times\left(\exp\left(\frac{\alpha_{ak} n_k F}{RT}\left(V_M - \Phi_{0a} - E_k\right)\right) - \exp\left(-\frac{\alpha_{ck} n_k F}{RT}\left(V_M - \Phi_{0c} - E_k\right)\right)\right) \tag{20}$$

Boundary Condition

The boundaries of the studied electrowinning cell include inlet, outlet, electrode surfaces and inner cell walls. The boundary conditions were evaluated assuming that the fluid flow is incompressible laminar flow (Re < 1,000). The grid was extended to store the values of the physical properties at the boundaries. The boundary conditions applied in the discretized equation via source term are described in the following sections.

Inlet Boundary Conditions

The distributions of all flow variables, except pressure, were specified at the inlet to the electrowinning cell. The flow direction was top nozzle to the bottom nozzle on the opposite side of cell as shown in Figure 4. Uniform initial conditions were assumed for Ci and T,

$$C_i = C_\infty \tag{21}$$

$$T = T_0 \tag{22}$$

On the fluid inlet boundary,

$$u_i = u_0 \tag{23}$$

$$C_i = C_{i\infty} \tag{24}$$

$$\frac{\partial \Phi}{\partial n} = 0 \tag{25}$$

Outlet boundary conditions

At the outlet boundary, the flow is directed out of the domain. The hydrodynamic boundary condition (i.e., mass and momentum) involves constraints on the boundary static pressure, velocity or mass flow. For all other transport equations, the outlet value of the variable is part of the solution.

In our model, zero gradients for all variables, except pressure, in the normal direction were assumed. On the fluid outlet boundary,

$$\frac{\partial C_i}{\partial n} = 0 \tag{26}$$

$$\frac{\partial \Phi}{\partial n} = 0 \tag{27}$$

Wall Boundary Conditions

In this modeling work, non-slip and non-penetrating wall conditions were assumed. The electrolyte velocity in the additional grid line was set to be zero (the grid line used for

implementation wall boundary conditions). Since there is no mass transfer of species through the cell wall, the gradient of the species concentration was set to zero, (∂Cw/∂n = 0). This was implemented by setting the values of the species concentration at the wall as the nearby cells.

The degree of electric current closure depends on the electric properties of the walls (thickness and conductivity). Consequently, various possible combinations of hydrodynamic and electromagnetic boundary conditions can be obtained depending on the thickness, electrical conductivity, and magnetic permeability of the walls. In the present work, only the electric properties are taken into consideration and the wall thickness is much smaller than the width and depth of the cell cavity. The conductivities of the walls of electrowinning cell are assumed to be zero, i.e. no electric current enters into the walls.

On insulating wall boundaries:

$$u_i = 0 \tag{28}$$

$$\frac{\partial C_i}{\partial n} = 0 \tag{29}$$

$$\frac{\partial \Phi}{\partial n} = 0 \tag{30}$$

Electrode Surface Boundary Conditions

On a cathode (+) or anode (-) surfaces, the interfacial flux of certain species should be equal to the generation or consumption of the species by the associated electrochemical reactions, i.e. the normal flux of reacting species is a sum of reaction currents (i_K), whereas for non-reacting species is zero. The conditions are given by:

Reacting species: $$-D_i \frac{\partial C_i}{\partial n} - z_i D_i C_i \frac{\partial \Phi}{\partial n} = (\pm 1) \sum_k \frac{s_{ik} i_k}{n_k} \tag{31}$$

Non-reacting species: $$-D_i \frac{\partial C_i}{\partial n} - z_i D_i C_i \frac{\partial \Phi}{\partial n} = 0 \tag{32}$$

The kinetic and thermodynamic parameters, species diffusion coefficients, and reference species concentrations used to solve this model are listed in
Table 45. The governing equations and associated boundary conditions were numerically solved using finite volume method which is discussed in the following section.

Implementation of Equations

In this research, the mathematical model is solved using Ansys CFX, which is a very flexible finite volume code widely used in the industrial applications. Customized user scalar equations can be introduced into the numerical scheme by user-defined subroutines. These routines include boundary conditions, coupled momentum equations with electromagnetic equations, and coupled species conservation equations with electrochemical kinetic equations, etc.

By default the electromagnetic equations are not included in CFX, certain modifications are made in order to include the effects of electromagnetic. This involves the solution of the electric potential equation using the additional scalar equation, and the coupling of potential equation with momentum equation. The electric potential and species boundary conditions also need special treatment to consider the electrochemical kinetics as shown in Eqns. 18-32.

Electrical Field Distribution

The results of the computation of the potential distribution and the electrical field showed that the electrical potential is distributed intensively between two separated electrodes and the main gradient exists around the edges of electrodes and induces electrolyte to flow from anode to cathode. Therefore, electric field intensity is high between the electrodes and almost zero in the cross region between electrodes and cell wall.

Concentration Profile

During the aluminum electrowinning in chloroaluminate ionic liquid electrolyte, the current is transported through the bath almost exclusively by the $Al_2Cl_7^-$ and $AlCl_4^-$ ions, whereas the cation $C_n$mim+ acted as supporting electrolyte. Concentration gradients were found to decrease from the upper part of cell to the inactive bottom part. The iso-concentration contour becomes steeper near the center of the electrodes. The higher concentration gradients on the outside of electrode surface are likely due to the presence of large inactive surface. This surface allows partial replenishment of the boundary layer by the diffusion of the electroactive species. It is also observed that the contours are smooth and even at the low Renolds number. In addition, the development of the concentration profile with increasing Renolds number was as expected. At the low Renold number, the concentration changes in the electrodes realm were mainly due to diffusion and migration. At greater Renolds number, the convection effects dominated and concentration changes were confined in to a smaller distance from the electrode surfaces, since the thickness of the mass transfer boundary layer was progressively reduced.

Current Density and Fluid Flow

The streamline calculation of electrolyte fluid flow at steady state showed the main flow pattern was several circulation cells in the bulk of the electrolyte. The formation of the circulation velocity is a consequence of the interaction between the velocity gradient and the applied electrical field. The impact on the flow is a Lorenz force opposing the fluid flow to accelerate or decelerate. Due to the significant increase in electrical potential gradient, it is expected that there are more intensive small circulation cell developed at the edges of electrodes.

The current density modeling are based on the electrical field and current density distribution calculation. The computed current density vector plots indicated that current flow from the anode through the electrolyte to the cathode, while it is nearly zero everywhere else. The streamtraces which are actually the paths of ions moving in the current field within the electrolyte correspond to the current line. The current density near the edges of electrode is generally more intensive

than elsewhere within the cross section. With varying electrode distance, the mean current density values Ψ within the cross section electrolyte domain changes. Under optimum electrode distance the mean current density (dimensionless) becomes maximum corresponding to the applied minimum cell voltage, where the electrolyte concentration, temperature and geometry of cell are set to constant. Our early modeling results on cylindrical electrowinning cell showed the relation between applied cell voltage and electrode distance with mean current density as a parameter when electrolyte temperature was 90^{o}C and concentration was 50 mol% of $AlCl_3$. The optimum electrode distance was determined to be ~1.5 cm when maximum mean current density was achieved with minimum applied cell voltage.

Based on the results of 3-D electrical field and current density modeling on electrowinning cell, the experimental data were compared with modeling results as shown in Figure 6. The modeling results were in good agreement with experimental data below 3.5 volts, but there was significant difference with applied cell voltages above 3.5 volts. This may be due to the cathodic side reactions are significant when cell voltage increases to higher than 3.5 volts. The electrochemical window of the studied ionic liquid electrolyte is between 2.2 to 4.0 volts. When the applied cell voltage approaches the maximum electrochemical cell voltage (window) of ionic liquid electrolyte, electrochemical properties of ionic liquid electrolyte may also experience abnormal behavior as observed in the discrepancy between our modeling and experimental results.

Electrowinning Cell Design Parameters

One of the major benefits of modeling work is to help design and optimize the electrowinning cell on multiple scales. In designing or developing any electrochemical reactors (cells, tanks), one must take into account the purpose of the reactor as well as the electrolyte properties and special features of the reactions involved in it. When designing the electrochemical reactor, several basic parameters need to be considered such as interelectrode distance, electrolyte flow condition and scale factors.

The relative electrolyte volume available per unit surface area of the electrodes is determined by the distance between the electrodes (d). This distance is usually between several millimeters and over 10 cm. The ohmic losses in the electrolyte increase with the distance between the electrodes. On the other hand, when the electrolyte volume is too less, the mass transfer and reactant concentrations will change rapidly. Figure 7 shows the effects of electrode surface area per unit volume on average current density for two different electrode configurations. It is obvious to see that a maximum average current density can be achieved at certain values of electrode distance when other variables are fixed. The maximum average current density is probably the result of decreasing the mass transfer resistance within the electrolyte as 1/d decreased (convection enhanced between electrodes). In our case, the electrolyte is pumped around in an external circuit with an additional electrolyte vessel. It is obvious that varying the distance between electrodes will affect the electrical field distribution over the extent of cell domain. Based on the electric field distribution calculation, optimum variables such as applied cell voltage and electrode distance were determined.

When scaling up the reactors to large-volumes, the electrode dimensions increases considerably (i.e. height and width) and the total current density is large, ohmic losses will become significant within the electrodes which lead to a non-uniform current-density distribution. Non-uniformity of the current density distribution in the electrolyte may cause stratification in the electrolyte solutions (i.e. electrolyte layers of lower density formed due to the reaction may move to the upper portion of the reactor, and denser electrolyte layers will stay in the lower portion of the reactor). This is particularly the case for large volume ionic liquid electrowinning reactors. Since ionic liquid electrolytes are generally more viscous than aqueous solution, the viscous drag body force in ionic liquid electrolyte usually is over one magnitude of order greater than that of aqueous media. Increasing the stirring or fluid flow condition can certainly help to alleviate this problem as shown in our modeling work. Further modeling research work are needed to better understand the potential scaling-up problem as mentioned above.

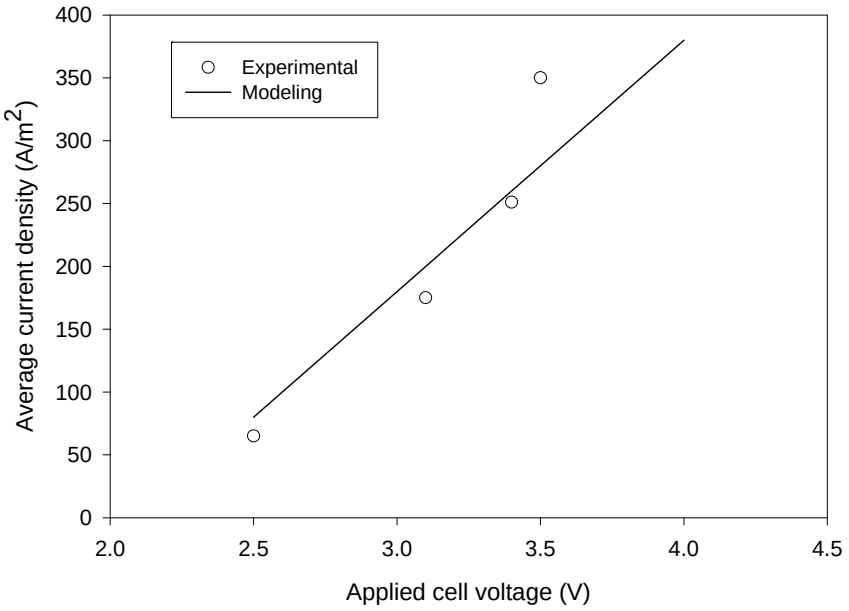

Figure 6. Voltage versus current curves, experimental and modeling results.

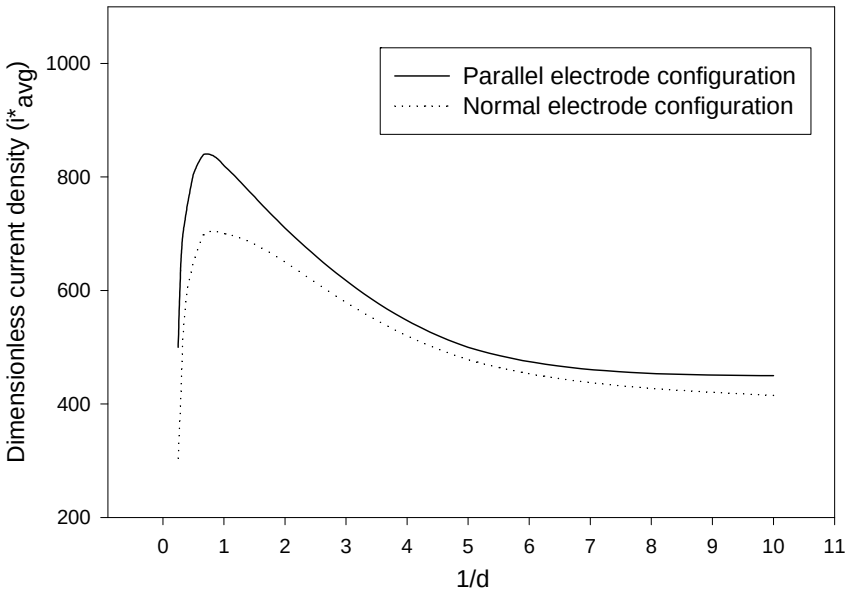

Figure 7. Effects of electrode surface area per unit volume (1/d) on average current density.

Hardware Requirement and Tools used in Simulation

1. Hardware

All the simulation and calculation were performed on a Dell Dimension DIM9100 installed with Microsoft Windows XP Professional (Version 2002, Service Pack 2). It features two processors, Intel(R) and Pentium(R), each CPU at 3.20GHz and 3.19GHz, and with 2.00 GB RAM.

2. Software

The commercial fluid dynamics software packages Ansys®10.0 and CFX®10.0 are used for solving the simulation problems.

- Preprocessing tool: Ansys® 10.0 and CFX®-Pre 10.0

Geometry setup and meshing: The geometry of electrochemical cell is created using Preprocessor-> Modeling tools integrated in Ansys. Firstly all blocks or volumes forming the computational domain are created. Then these blocks and volumes are moved, glued or merged together using Boolean operation. The components and patches (parts of domain where the boundary conditions will be defined – such as walls, inlet, outlet etc.) are specified by grouping components of the domain. Grid generation tool (meshing tool) in Ansys is used to create non-uniform grids (grids of boundary layers are refined).

- Solver: CFX®-Solver 10.0

The basis of the code is a conservative finite volume method. All variable are defined at the center of control volumes, and the equations are integrated over each control volume to obtain

discrete equations. The complete set of equations is solved by iterative method. Pressure-correction algorithm is used to ensure mass conservation.

- Postprocessing tool: CFX®-Post 10.0

The integrated graphic post processor in CFX 10.0 is used for analysis and presentation of results obtained from the solver. In addition to CFX, the following software tools are used for data acquisition and processing, subroutine programming.

Compaq Visual Fortran 6.6A – It is used for compilation of the user subroutines that are called by the CFX solver. Additional Fortran subroutines are utilized to implement the customized boundary conditions, momentum and mass sources. They are also used to solve the user scalar equations, specify variable boundary conditions and set up converging criteria.

Matlab, OriginLab and Sigmaplot 2000 – Besides CFX Post tool, these graphic or programming tools are used to visualize the solution results.

Computer Model Code (ANSYS and CFX Command Files)

The command files for ANSYS and CFX operations used during the simulation are presented, which include 3D geometry of electrowinning cell, meshing of the computational domain, initial/boundary condition setup.

```
!*
/NOPR   ! Suppress printing of UNDO process
/PMACRO ! Echo following commands to log
FINISH  ! Make sure we are at BEGIN level
/CLEAR,NOSTART  ! Clear model since no SAVE found
! 3D electrowinning cell geometry setup for parallel-configured electrodes
/input,start90,ans,'C:\Program Files\Ansys Inc\v90\ANSYS\apdl\',,,,,,,,,,,,,,,1
/REPLOT,RESIZE
!*
/NOPR
/PMETH,OFF,0
KEYW,PR_SET,1
KEYW,PR_STRUC,0
KEYW,PR_THERM,0
KEYW,PR_FLUID,0
KEYW,PR_ELMAG,1
KEYW,MAGNOD,0
KEYW,MAGEDG,0
KEYW,MAGHFE,0
KEYW,MAGELC,0
KEYW,PR_MULTI,1
KEYW,PR_CFD,1
```

```
/GO
!*
/VERIFY,3DBatchEMAGclindrical
/PREP7
/TITLE, 3DBatchEMAGcylindrical, STEADY STATE EMAG ANALYSIS IN CYLINDRICAL CELL
ANTYPE,STATIC              ! STATIC ANALYSIS
ET,1,FLUID142
MPTEMP,,,,,,,,
MPTEMP,1,0
MPDATA,DENS,1,,1234
MPTEMP,,,,,,,,
MPTEMP,1,0
MPDATA,VISC,1,,2.7
CYL4,0,0,4.3, , , ,10
LWPL,-1,10,0
wpro,,,90.000000
FLST,2,1,8
FITEM,2,4.1,0,7
WPAVE,P51X
FLST,2,1,8
FITEM,2,4.1,0,9
WPAVE,P51X
CONE,0.5,0.2,0,2,0,360,
FLST,3,1,6,ORDE,1
FITEM,3,2
VSYMM,X,P51X, , , ,0,0
FLST,3,1,6,ORDE,1
FITEM,3,3
VGEN, ,P51X, , ,0,0,-6, , ,1
FLST,2,3,6,ORDE,2
FITEM,2,1
FITEM,2,-3
VADD,P51X

WPAVE,0,0,0
CSYS,0
WPSTYLE,,,,,,,,1
wpro,-270,,180
BLOCK,-2,2,1.5,1.7,0,-7,
BLOCK,-2,2,-1.5,-1.7,0,-7,
vlist, all
VSBV,      4,      1
FLST,2,2,6,ORDE,2
FITEM,2,2
FITEM,2,-3
```

```
vlist, all
VSBV,      3,      2
alist, all
CM,_Y,VOLU
VSEL, , , ,      1
CM,_Y1,VOLU
CMSEL,S,_Y
!*
CMSEL,S,_Y1
VATT,      1, ,   1,      0
CMSEL,S,_Y
CMDELE,_Y
CMDELE,_Y1
!*
MPTEMP,,,,,,,,
MPTEMP,1,0
MPDE,DENS,1
MPDATA,DENS,1,,0.001234
MPTEMP,,,,,,,,
MPTEMP,1,0
MPDE,VISC,1
MPDATA,VISC,1,,0.000027
MPTEMP,,,,,,,,
MPTEMP,1,0
MPDE,DENS,1
MPDATA,DENS,1,,0.001234
MPTEMP,,,,,,,,
MPTEMP,1,0
MPDE,VISC,1
MPDATA,VISC,1,,2.7E-005
!*
MPTEMP,,,,,,,,
MPTEMP,1,0
MPDE,DENS,1
MPDATA,DENS,1,,0.001234
ESIZE,0.3,0,
MSHAPE,1,3D
MSHKEY,0
!*
CM,_Y,VOLU
VSEL, , , ,      1
CM,_Y1,VOLU
CHKMSH,'VOLU'
CMSEL,S,_Y
!*
VMESH,_Y1
```

```
!*
CMDELE,_Y
CMDELE,_Y1
CMDELE,_Y2
!*
/UI,MESH,OFF
TUNIF,373,
FLST,5,1,5,ORDE,1
FITEM,5,10
CM,_Y,AREA
ASEL,R, , ,P51X
CM,_Y1,AREA
CMSEL,S,_Y
CMDELE,_Y
!*
FLST,5,1,5,ORDE,1
FITEM,5,10
CM,_Y,AREA
ASEL,R, , ,P51X
CM,_Y1,AREA
CMSEL,S,_Y
CMDELE,_Y
!*
DA,_Y1,VX,0.5,1
DA,_Y1,VY,0,1
DA,_Y1,VZ,0,1
!*
CMDELE,_Y1
!*
/VIEW,  1, -0.209889982529    ,  0.648632665594    , -0.731588586815
/ANG,   1,   179.574461050
/REPLO
/VIEW,  1, -0.723493237334E-01,  0.852620765957    , -0.517497251020
/ANG,   1,   173.815330338
/REPLO
alist, all
FLST,5,18,5,ORDE,8
FITEM,5,1
FITEM,5,-3
FITEM,5,5
FITEM,5,7
FITEM,5,-9
FITEM,5,11
FITEM,5,13
FITEM,5,-22
CM,_Y,AREA
```

```
ASEL,R, , ,P51X
CM,_Y1,AREA
CMSEL,S,_Y
CMDELE,_Y
!*
!*
DA,_Y1,VX,0,1
DA,_Y1,VY,0,1
DA,_Y1,VZ,0,1
!*
CMDELE,_Y1
!*
FLST,5,1,5,ORDE,1
FITEM,5,6
CM,_Y,AREA
ASEL,R, , ,P51X
CM,_Y1,AREA
CMSEL,S,_Y
CMDELE,_Y
!*
/GO
!*
DA,_Y1,PRES,0,1
!*
CMDELE,_Y1
!*
DALIS, ALL
FINISH
/SOL
FLDATA2,ITER,EXEC,20,
FLDATA2,ITER,OVER,0,
FLDATA2,ITER,APPE,0,
FLDATA3,TERM,VX,0.01,
FLDATA3,TERM,VY,0.01,
FLDATA3,TERM,VZ,0.01,
FLDATA3,TERM,PRES,1e-008,
FLDATA3,TERM,TEMP,1e-008,
FLDATA3,TERM,ENKE,0.01,
FLDATA3,TERM,ENDS,0.01,
FLDATA5,OUTP,SUMF,10,
!*
FLDATA5,OUTP,DEBG,1
FLDATA5,OUTP,DRAD,0
FLDATA6,CONV,OUTP,LAND
FLDATA6,CONV,ITER,1,
!*
```

```
FLDATA12,PROP,DENS,2
FLDATA13,VARY,DENS,0
FLDATA12,PROP,VISC,2
FLDATA13,VARY,VISC,0
FLDATA12,PROP,COND,0
FLDATA13,VARY,COND,0
FLDATA12,PROP,SPHT,0
FLDATA13,VARY,SPHT,0
!*
FLDATA7,PROT,DENS,LIQUID
FLDATA8,NOMI,DENS,0.001234,
FLDATA9,COF1,DENS,0,
FLDATA10,COF2,DENS,0,
FLDATA11,COF3,DENS,0,
FLDATA7,PROT,VISC,LIQUID
FLDATA8,NOMI,VISC,0.000027,
FLDATA9,COF1,VISC,0,
FLDATA10,COF2,VISC,0,
FLDATA11,COF3,VISC,0,
FLDATA12,PROP,IVIS
FLDATA7,PROT,COND,CONSTANT
FLDATA8,NOMI,COND,1,
FLDATA9,COF1,COND,0
FLDATA10,COF2,COND,0
FLDATA11,COF3,COND,0
FLDATA7,PROT,SPHT,CONSTANT
FLDATA8,NOMI,SPHT,-1,
FLDATA9,COF1,SPHT,0
FLDATA10,COF2,SPHT,0
FLDATA11,COF3,SPHT,0
!*
FLDATA15,PRES,REFE,1013.25,
FLDATA16,BULK,BETA,1e+015,
FLDATA17,GAMM,COMP,1.4,
FLDATA14,TEMP,NOMI,293,
FLDATA14,TEMP,TTOT,373,
FLDATA14,TEMP,BULK,373,
TOFFSET,0,
!*
ACEL,0,0,981,
)/GOP    ! Resume printing after UNDO process
```